Indoor Positioning of a Robotic Walking Assistant for Large Public Environments

Payam Nazemzadeh[1], Federico Moro[1], Daniele Fontanelli[2], David Macii[2], Luigi Palopoli[1] [1]Dep. of Information Engineering and Computer Science, University of Trento, Trento, Italy
[2]Dep. of Industrial Engineering, University of Trento, Trento, Italy
E–mail: {payam.nazemzadeh,daniele.fontanelli,david.macii}@unitn.it, {moro,palopoli}@disi.unitn.it

***Abstract*—Indoor localization and position tracking are essential to support applications and services for Ambient Assisted Living (AAL). While the problem of indoor localization is still open and already quite complex per se, in large public places additional issues of cost, accuracy and scalability arise. In this paper the position estimation and tracking technique developed within the project "Devices for Assisted Living" (DALi) is described, analyzed through simulations and finally validated by means of a variety of experiments on the field. The goal of the DALi project is to design a robotic wheeled walker guiding people with psychomotor problems. Indeed, people with motor or cognitive impairments are often afraid of moving in large and crowded environments (e.g. because they could lose the sense of direction). In order to mitigate this problem, the position tracking approach described in this paper is based on multi-sensor data fusion and it is conceived to assure a good trade-off between target accuracy, level of confidence and deployment costs. Quite interestingly, the same approach could be used for indoor automated guided vehicles (AGV) and robotics.**

***Keywords*—Assistive devices, position measurement, navigation, Kalman filtering, sensor fusion, performance evaluation.**

I. Introduction

According to recent market forecasts and analyses, the worldwide turnover related to indoor navigation is expected to reach 2.6 billion dollars in 2018 at a compounded annual growth rate (CAGR) of about 42% [1]. The range of potential applications of indoor localization is very large. One of the most interesting is the so-called *Ambient Assisted Living* (AAL), i.e. the application of information and communication technologies (ICT) to the assistance of older adults or of people with impairments. In this field, most of the challenges come from the fragility of users and from their specific state of mind. In order to be applicable in AAL, a localization technology has to be robust, reliable and, most importantly, acceptable for the user [2].

The project *Devices for Assisted Living* (DALi) is an EU research initiative with the goal of developing a wheeled robotic assistant (called *c-Walker*) able to offer a concrete support to older adults in their navigation within complex indoor environments, such as shopping malls, railway stations or airports. The c-Walker helps the user decide a route in the environment (e.g. to visit a sequence of desired locations), monitors the surroundings to detect possible anomalies or hazards, adapts the path to the changing conditions of the environment, and guides the user along the path by using electromechanical brakes or haptic interfaces. Such tasks rely on accurate real–time position estimation, which is the specific topic of this work.

Although the c-Walker is the outcome of a particular research project, the position tracking approach is applicable to a much larger class of service robots offering "close" assistance to their users. In particular: i) the wanted accuracy and the related level of confidence have to be good enough to enable fine-grained corrections and maneuver in confined spaces; ii) the cost of the device and the impact of the instrumentation in the environment should be reasonable both for common users and for the managers of the public space; iii) the form factor of the walker has to be acceptable in terms of size, weight and invasiveness; iv) the proposed approach has to be scalable enough to allow the operation of several walkers at the same time. All these requirements cannot be met by using just a single localization technique. For instance, the positioning uncertainty of solutions based on radio signal strength intensity (RSSI) measurements and fingerprinting can be so large as a few meters, which is inadequate for the intended purpose [3], [4], [5].

Techniques based on round-trip time (RTT) or time-of-arrival (ToA) measurements of Ultra Wide-Band (UWB) [6], [7], Chirp Spread Spectrum (CSS) [8], [9], [10], or ultrasonic signals [11], [12], even if accurate in line-of-sight (LOS) conditions, could be severely affected by fixed or moving obstacles, which are quite common in large public (and potentially crowded) environments. Moreover, the use of constantly active wireless links between the moving target and multiple fixed "anchor" nodes is hardly scalable and poses interference problems when multiple objects have to be tracked at the same time. Also, the measurement data collected by different nodes should be properly synchronized through an ad-hoc protocol, which may pose reliability and bandwidth issues [10], [13].

The use of wearable inertial measurements units (IMU) installed either on shoes or on portable items for pedestrians [14], [15], [16], is possible in principle, but its efficacy for people with deambulation problems is questionable.

Finally, the position tracking techniques based exclusively on vision systems, even if precise, generally require powerful and expensive computational platforms [17], [18]. Moreover, the use of cameras is influenced by light conditions and may pose range, privacy and scalability issues.

doi: 10.1109/TIM.2015.2437637

In order to tackle the manifold issues listed above, many researchers nowadays think that the best approaches for high-performance and scalable indoor positioning should rely on multi-sensor data fusion [19], [20]. This is also the approach described in this paper. When a walking assistant, like the DALi's c-Walker, is used, odometry and gyroscopes data can be combined with *sporadic* external measurement results providing information on absolute position and direction of motion [21].

In the rest of this paper, at first in Section II some related work is presented to emphasize similarities and differences between the proposed technique and other solutions found in the literature. In Section III the localization problem is formulated and the underlying system and measurement models are described. Such models partially derive from the results of preliminary studies reported in [22] and [23], but they have been improved in order to estimate and to compensate the effect of possible left-side/right-side mechanical asymmetries of the device. Section IV is focused on the description of the chosen estimator. Section V reports some simulation results based on the data collected from real sensors. The purpose of the simulations is to analyze the behavior of the position tracking technique in different conditions to achieve a suboptimal trade-off between performances and deployment costs. Such results are partially different from those reported in [21], because they are based on a better characterization of the sensors actually used in the development of the c-Walker. Section VI deals with a short description of the c-Walker prototype and includes the results of a variety of on-the-field experiments. Finally, Section VII concludes the paper.

II. Related Work

The results of the experimental activities reported in [31] confirmed that the accuracy of high-performance wireless ranging techniques is quite limited in non-LOS conditions. Thereby, a number of alternative approaches (in part borrowed from robotics) have been considered to fulfill the multi-faceted requirements described in Section I. A list of the main research works that inspired the proposed approach, along with a short description of their advantages and disadvantages, is summarized in Table I.

First of all, since we deal with the localization of a wheeled device, a powerful resource for positioning is offered by odometry. However, as customary of dead reckoning techniques, odometry-based localization suffers from unbounded uncertainty growth and lack of initial observability. While position and orientation errors generally increase with a rate depending on both odometer resolution and accuracy, estimation results can be considerably improved by fusing gyroscope and encoder data on the basis of their respective uncertainties in different conditions of motion [24]. Unfortunately, also in this case there are no guarantees to keep the overall position uncertainty bounded. Moreover, the initial state of the system is still unobservable. To tackle these problems, an additional absolute localization technique is certainly needed. Given that no external wireless ranging solutions based on RSSI or ToF measurements proved to be accurate enough [31], the absolute position values can be obtained from a set of passive RFID tags. In fact, they are inexpensive, can be stuck on the floor at known locations, and, even if they have a quite limited range (in the order of a few tens of cm or less), they can be easily detected, regardless of the number of people and obstacles in the environment. Four good solutions of this kind are described in [25], [26], [27], [28]. In [25] a fine-grained grid of passive RFID tags is used for robot navigation and trajectory reconstruction. No other sensors are employed. In [26] a similar approach is adopted, but an additional vision system is used to recognize the color patches placed on the top of different robots. In [27] a similar grid of RFID tags is used along with a set of ultrasonic sensors installed on the front side of a robot for position refinement through data fusion. A common characteristic of the solutions mentioned above is high accuracy, which however is paid in terms of RFID grid granularity. In fact, in all cases the grids of tags are very dense (with distances between about 0.3 m and 0.5 m), which is costly and impractical in very large environments. Moreover, the fixed external cameras in [26] pose privacy and scalability issues, while the on-board ultrasonic sensors (which refine position in the presence of fixed obstacles) could lead to unpredictable results in densely populated environments. In [28] the problem of RFID density is partially addressed by a special triangular multiloop-bridge reader antenna that generates voltage signals across a bridge circuit. Since such signals are a function of tag location, by combining them with both the information from a database and the data measured by the encoders of a wheeled device (e.g. a wheel-chair), the position and the orientation of the device can be estimated with high accuracy and with a smaller number of RFID tags.

In this paper our goal is not to maximize accuracy, but rather to assure a good compromise between accuracy, level of confidence, costs and deployment complexity. A similar idea is described also in [29] that, to the best of our knowledge, is the research work closest to the solution presented in this paper. In [29] a smart walker instrumented with encoders, a compass and an RFID reader corrects the odometry-based position by reading mats of RFID tags placed in strategic points of corridors (i.e. where people are supposed to come across with a high probability). However, that solution suffers from some drawbacks. First of all, the use of mats is not suitable for wide rooms where the user can potentially move in any direction. Secondly, the adopted sensor fusion algorithm is unclear. Apparently, the sensors measurement uncertainties are not used to support the estimation model, as instead it is done in this work. Thirdly, the problem of attitude estimation is addressed with a compass that, in our experience, can lead to very poor results in some indoor environments. In this respect, it is worth emphasizing that the long-term position uncertainty is crucially affected not only by the accuracy of the absolute localization system, but also by possible attitude or orientation errors. Even assuming that the coordinates of the moving target are perfectly adjusted when an RFID tag is detected, the position error may grow quickly if the estimated orientation is very different from the real one. This problem is not so visible when the RFID grid is dense, but it becomes significant when

TABLE I. MAIN FEATURES OF VARIOUS POSITION TRACKING TECHNIQUES THAT INSPIRED THE APPROACH PROPOSED IN THIS PAPER.

Paper	Highlights	Pros	Cons
De Cecco [24]	- Odometry and Gyroscope - Sensor data fusion depends on their uncertainties in different conditions of motion	- Very accurate after calibration	- Initialization required - Bounded positioning uncertainty is not guaranteed in the long run
Park et al. [25]	- Passive RFIDs only - At least one RFID must be read at every sampling time - Position computed through an incremental trigonometric approach	- Absolute localization - No other sensors are needed	- Large number of RFID tags - Tested at very low speeds (12 cm/s)
Choi et al. [26]	- Fusion of active sensing and passive RFID reads - Cameras on the ceiling to detect the position of the robot	- Absolute localization - Accurate	- Large number of RFIDs - It relies on external cameras - Difficult to use in large rooms
Choi et al. [27]	- Combines global RFID-based positioning with local ultrasound-based distance measurements	- Absolute localization - Very accurate	- Large number of RFID tags - Position refinement difficult in spaces with moving obstacles.
Ahmad et al. [28]	- A special triangular multiloop-bridge reader antenna generates signals that are a function of tag location. - Voltage signals are combined with information from database and with encoder data.	- Coarser RFID tag grid granularity - High accuracy	- Maximum distance between RFID tags still too limited (about 130 cm)
Kulyukin et al. [29]	- Use of encoders - Position correction through RFID mats	- Absolute localization - Mats are easy to deploy and they can be sparse (due to the use of encoders)	- Works well in corridors, but not suitable in large rooms - Unclear data fusion technique - Compass not always suitable in indoor environments
Nazari et al. [30]	- Carpets of passive RFID - Four RFID readers - Position and orientation estimates based on simultaneous label detection	- Absolute localization - Accurate - Focus not only on positioning, but also on orientation estimates	- Large number of RFID tags - Four RFID readers on the vehicle

RFID grid granularity is coarse. In such cases, an additional sensing system able to measure the orientation of the walker in a global reference frame is needed, as it is confirmed by the analysis reported in [22]. This result is also consistent with the solution described in [30], where, in order to estimate the orientation of a mobile device over a carpet of RFID tags, four RFID readers are used to detect at least two tags at a time. Unfortunately, in our case adding too many readers would make the walker bulky, fragile and uncomfortable for the user. In addition, the distance between pairs of adjacent tags should be small enough to enable the detection of two tags at a time, thus making, again, the grid quite dense. Since compasses and magnetometers proved to be quite unreliable indoors, we decided to measure the walker's orientation by means of a low-cost front camera already available on the device for collision avoidance and trajectory planning. In particular, the camera is supposed to detect suitable markers (e.g. arrow-shaped adhesive stickers) deployed in the environment. Even if such markers could be aesthetically unpleasant in some contexts, the use of a standard and properly chosen type of markers makes the performance of the localization system more robust to changeable environmental conditions. Moreover, in spite of the typical problems that may arise when a vision system is employed in potentially crowded environments (e.g. due to obstacles), we think that cameras can still be very effective for the intended purpose, provided that the following conditions hold, i.e. i) the visual markers pointing towards a known direction are easy and unambiguous to detect; ii) the camera duty cycle is kept as low as possible (e.g. it is activated every few seconds) and iii) the image processing algorithm is simple, robust and computationally light.

III. PROBLEM FORMULATION

A qualitative overview of the framework underlying the proposed position estimation technique is shown in Fig. 1(a)-(b). In principle, the motion of a wheeled walker in a reference frame $\langle W \rangle = X_w \times Y_w \times Z_w$ can be described by the following basic kinematic system, i.e.

$$\dot{\mathbf{s}} = \begin{bmatrix} \dot{x} \\ \dot{y} \\ \dot{\theta} \end{bmatrix} = \begin{bmatrix} v\cos\theta - L\omega\sin\theta \\ v\sin\theta + L\omega\cos\theta \\ \omega \end{bmatrix}, \quad (1)$$

$$\mathbf{o} = \mathbf{s}, \quad (2)$$

where $\mathbf{s} = [x,\, y,\, \theta]^T$ is the vector of the state variables, v is the forward velocity of the walker along the direction of motion, ω is its angular velocity, L is a constant representing the minimum distance between the mid–points of the rear and front wheels, respectively, and $\mathbf{o}$ is the output vector of the system. Notice that $(x,\, y)$ in Fig. 1(a) are the Cartesian coordinates of the mid–point of the front wheel axle on plane $X_w \times Y_w$, while θ is the walker's orientation angle. This angle is defined by the longitudinal axis of symmetry of the walker with respect to axis X_w, as shown in Fig. 1(b). Since the walker acts as a unicycle–like vehicle, the forward and angular velocities, v and ω, can be regarded as functions of the rear wheel velocities, i.e. $v = \frac{r}{2}(\omega_r + \omega_l)$ and $\omega = \frac{r}{d}(\omega_r - \omega_l)$, where ω_r and ω_l are the angular velocities of the right and

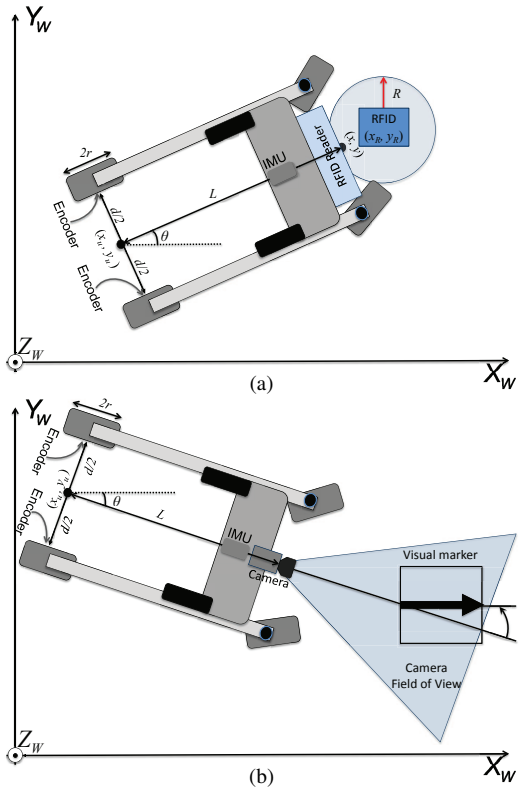

Fig. 1. Qualitative overview of the walker's position estimation problem, with a special emphasis on RFID tag detection (a) and visual marker recognition (b).

left wheel, respectively, r is wheel radius and d is the rear axle length. Ideally, once the initial position and orientation of the walker are known, measuring v and ω over time would be sufficient to reconstruct its position. However, both random and systematic measurement contributions tend to accumulate, thus leading to poor accuracy in the long run. Therefore, in order to mitigate this problem, such contributions should be properly included in the system model and they should be also taken into account by the chosen estimator. Observe that the state variables in $\mathbf{s}$ refer to the mid-point of the front wheels, which is the position where both the camera and the RFID are installed. However, in practice we are mainly interested in the position (x_u, y_u) of the human pushing the walker. Assuming that his/her centroid is reasonably aligned with the mid-point of the rear wheels, the following transformation holds, i.e.

$$\begin{bmatrix} x_u \\ y_u \end{bmatrix} = \begin{bmatrix} x - L\cos\theta \\ y - L\sin\theta \end{bmatrix}. \tag{3}$$

Therefore, the localization problem described in this paper has two complementary objectives, i.e.

- estimating the coordinates (x_u, y_u) of the human with a root mean square (RMS) euclidean error no larger than $\eta_p$with at least α_p probability;
- estimating the walker's orientation angle θ with a RMS error no larger than η_o with at least α_o probability.

A. System description

In nonideal conditions, the system model should explicitly take into account those phenomena (such as undetected encoder pulses, slight differences in wheels radius, mechanical asymmetries, noise) which make position and orientation uncertainty grow indefinitely. As a result, the continuous-time system model (1) can be changed as follows, i.e.

$$\dot{\mathbf{s}}' = \begin{bmatrix} \dot{x} \\ \dot{y} \\ \dot{\theta} \\ \dot{\mu} \\ \dot{\delta} \end{bmatrix} = \begin{bmatrix} (1+\mu)v\cos\theta - L\omega(1+\delta)\sin\theta \\ (1+\mu)v\sin\theta + L\omega(1+\delta)\cos\theta \\ \omega(1+\delta) \\ \gamma_\mu \\ \gamma_\delta \end{bmatrix}, \tag{4}$$

where the state vector $\mathbf{s}'$ comprises not only $\mathbf{s}$, but also the additional variables μ and δ. These represent the relative systematic offsets between the forward and angular velocity values at a given time and the respective odometry-based values. Observe that the time evolution of μ and δ relies on functions γ_μ and γ_δ, which depend on specific features of the system considered and should be determined through a proper experimental characterization. For instance, if in (5) $\gamma_\mu = \gamma_\delta = 0$, then μ and δ are just constant coefficients. System (4) can be conveniently expressed as a function of the angular velocity of the rear wheels, i.e.

$$\dot{\mathbf{s}}' = \mathbf{g}(\mathbf{s}')\boldsymbol{\Omega} + H\boldsymbol{\Gamma}, \tag{5}$$

where $\boldsymbol{\Omega} = [\omega_r, \omega_l]^T$, $\boldsymbol{\Gamma} = [\gamma_\mu, \gamma_\delta]^T$,

$$\mathbf{g}(\mathbf{s}') = \begin{bmatrix} c_\mu\cos\theta - Lc_\delta\sin\theta & c_\mu\cos\theta + Lc_\delta\sin\theta \\ c_\mu\sin\theta + Lc_\delta\cos\theta & c_\mu\sin\theta - Lc_\delta\cos\theta \\ c_\delta & -c_\delta \\ 0 & 0 \\ 0 & 0 \end{bmatrix},$$

$c_\mu = \frac{r}{2}(1+\mu)$, $c_\delta = \frac{r}{d}(1+\delta)$, $H = [\mathbf{0}_{2,3}, I_2]^T$, $\mathbf{0}_{m,n}$ is a $m \times n$ matrix filled with zeros and I_n is the identity matrix of dimension n. Note that $\mathbf{g}(\cdot)$ in (5) is a nonlinear vector function of the state. If (5) is discretized with sampling period T_s, the corresponding discrete-time system becomes

$$\mathbf{s}'_{k+1} = \mathbf{s}'_k + \mathbf{g}(\mathbf{s}'_k)\boldsymbol{\Delta\Phi}_k + T_s H\boldsymbol{\Gamma}, \tag{6}$$

where $\mathbf{s}'_k$ denotes the state vector at time kT_s and $\boldsymbol{\Delta\Phi}_k = \boldsymbol{\Omega}_k T_s = [\Delta\Phi_{r_k}, \Delta\Phi_{l_k}]^T$ is the vector of the angle displacements of the left and right wheels between kT_s and $(k+1)T_s$. Of course, the measured values of $\boldsymbol{\Delta\Phi}_k$ are generally affected by zero-mean random fluctuations $\boldsymbol{\epsilon}_k = [\epsilon_{r_k}, \epsilon_{l_k}]^T$ due to, for instance, vibrations, electronic noise and finite encoder resolution. Such random uncertainty contributions can be reasonably assumed to be independent. Therefore, (6) can be changed as follows, i.e.

$$\begin{aligned} \mathbf{s}'_{k+1} &= \mathbf{s}'_k + \mathbf{g}(\mathbf{s}'_k)(\boldsymbol{\Delta\Phi}_k + \boldsymbol{\epsilon}_k) + T_s H\boldsymbol{\Gamma} \\ &= \mathbf{s}'_k + \mathbf{g}(\mathbf{s}'_k)\widehat{\boldsymbol{\Delta\Phi}}_k + T_s H\boldsymbol{\Gamma}, \end{aligned} \tag{7}$$

where $\widehat{\boldsymbol{\Delta\Phi}}_k = [\widehat{\Delta\Phi}_{r_k}, \widehat{\Delta\Phi}_{l_k}]^T$ is the vector of the angle displacements measured between time kT_s and time $(k+1)T_s$.

B. Measurement model description

As shown in (2), the output vector $\mathbf{o}_k$ of the system in principle should be equal to $\mathbf{s}_k$. However, in practice not all output quantities can be measured at every sampling time.

As explained in Section II, the c-Walker is equipped with two encoders, a short-range RFID reader, a gyroscope and a front camera. While encoders and gyroscope can collect data at a rate equal to $1/T_s$, the RFID reader and the camera can detect a tag or a marker only if they are within their respective reading range. The ID code of each tag corresponds to known coordinates in $\langle W \rangle$, as shown in Fig. 1(a). However, no information about orientation is provided, since this generally cannot be measured through a single tag detection, unless special antennas are used [28].

To solve this problem, the orientation angle is estimated by using both the gyroscope available inside an Inertial Measurement Platform (IMU), and the orientation data extracted from the images collected from the camera, as shown in Fig. 1(b). In fact, the relative orientation angle with respect to a given initial value could be easily obtained by integrating the angular velocity of the walker around axis Z_w. However, the initial orientation is not observable and, in addition, the noise of the gyroscope also accumulates, thus causing potentially large random walk fluctuations in the long run. This problem could be addressed through a plain monodimensional Kalman Filter. The process noise of this filter can be assumed to have zero-mean and standard deviation $\sigma_{\omega_k} = a|\omega_{z_k}| + b$, where ω_{z_k} is the angular velocity measured by the gyroscope at time kT_s, while a and b are constant coefficients. This non-stationary model results from experimental evidence. In fact, several tests performed on real gyroscopes using an orbital rotator Stuart SB3 at various speeds in the range [2-40] rpm showed that the standard deviation of the gyroscope's noise tends to grow linearly with the rotational speed. Thus, the values of coefficients a and b can be easily estimated through a linear fitting.

Using this model, the prediction equations of the Kalman filter can be concisely written as follows, i.e.

$$\bar{\theta}^{+}_{k+1} = \bar{\theta}_k + T_s\omega_{z_k} \text{ and } \sigma^{2^+}_{\theta_{k+1}} = \sigma^2_{\theta_k} + T_s^2\sigma^2_{\omega_k}, \quad (8)$$

where $\cdot^+$ denotes prediction, $\bar{\theta}_k$ is the angle estimated at time kT_s (not to be confused with the homonymous state variable in $\mathbf{s}'_k$) and $\sigma^2_{\theta_k}$ is its variance. If no visual markers are in the field of view of the camera (as it is supposed to happen most times), then the Kalman filter is updated just using the predicted values, i.e. $\bar{\theta}_{k+1} = \bar{\theta}^{+}_{k+1}$ and $\sigma^2_{\theta_{k+1}} = \sigma^{2^+}_{\theta_{k+1}}$. If instead a visual marker is detected, the corresponding frame is turned into a top-view image through the so-called Inverse Perspective Mapping (IPM) [32]. Since the features of interest of the detected marker (e.g. an arrow) is associated with the direction of axis X_w, the orientation of the walker with respect to X_w is given by the angle between the line bisecting longitudinally the top-view image and the direction of the detected marker, as shown in Fig. 1(b). As a result, the orientation angle and its variance are updated as follows, i.e.

$$\bar{\theta}_{k+1} = \bar{\theta}^{+}_{k+1} + \frac{\sigma^{2^+}_{\theta_{k+1}}(\theta^c_{k+1} - \bar{\theta}_{k+1})}{\sigma^{2^+}_{\theta_{k+1}} + \sigma^2_{\theta^c_{k+1}}}, \quad (9)$$

$$\sigma^2_{\theta_{k+1}} = \frac{\sigma^2_{\theta^c_{k+1}}\sigma^{2^+}_{\theta_{k+1}}}{\sigma^{2^+}_{\theta_{k+1}} + \sigma^2_{\theta^c_{k+1}}}, \quad (10)$$

where θ^c_{k+1} and $\sigma^2_{\theta^c_{k+1}}$ denote the angle measured by the camera-based system and its variance at time $(k+1)T_s$, respectively.

In conclusion, the overall measurement model is

$$\mathbf{o}_k = C_k\mathbf{s}'_k + \boldsymbol{\zeta}_k, \quad (11)$$

where the output vector $\mathbf{o}_k$, the output matrix C_k and the vector $\boldsymbol{\zeta}_k$ of the measurement uncertainty contributions depend on what sensor data are actually available at time kT_s. Evidently, the elements of $\boldsymbol{\zeta}_k$ can be regarded as independent, as they are related to completely different sensors. Thus, the covariance matrix D_k associated with $\boldsymbol{\zeta}_k$ is diagonal.

Ultimately, two scenarios are possible.

- If no RFID tags are detected, then $C_k = [0 \;\; 0 \;\; 1 \;\; 0 \;\; 0]$ and $D_k = \sigma^2_{\theta_k}$. This is the variance of the orientation angle estimated through the Kalman filter described above.
- If instead an RFID tag is detected, then

$$C_k = \begin{bmatrix} 1 & 0 & 0 & 0 & 0 \\ 0 & 1 & 0 & 0 & 0 \\ 0 & 0 & 1 & 0 & 0 \end{bmatrix} \text{ and } D_k = \begin{bmatrix} \sigma^2_{x_k} & 0 & 0 \\ 0 & \sigma^2_{y_k} & 0 \\ 0 & 0 & \sigma^2_{\theta_k} \end{bmatrix} \quad (12)$$

  where $\sigma^2_{\theta_k}$ is, again, the variance of the angle estimated with the previous Kalman Filter, while $\sigma^2_{x_k}$ and $\sigma^2_{y_k}$ are the variances of the offsets between the nominal coordinates of the detected tag and the actual coordinates of the walker along axes X_w and Y_w. Assuming, to a first approximation, that the probability of reading a tag is constant within the circle centered in the tag itself and with radius R equal to the maximum nominal range of the RFID reader, then the uncertainty contributions associated with coordinates x and y are uncorrelated and $\sigma^2_{x_k} = \sigma^2_{y_k} = \frac{R^2}{4}$ [23].

IV. Walker position estimation and tracking

In general, the state of a nonlinear system can be efficiently estimated by an Extended Kalman Filter (EKF) under the assumptions that i) the system and output model nonlinearities are quite smooth and ii) the various uncertainty contributions are normally distributed with a zero mean. Since the potential non-zero relative velocity offsets modeling encoders imperfections are now explicitly included in the system, possible harmful biases can be introduced only by the RFID-based position measurements and/or by the camera-based or gyroscope-based angular measurements. However, in the domain of all possible trajectories, the mean values of such uncertainty contributions can be reasonably assumed to be zero. Also, their distribution

generally exhibits a quite Gaussian behavior [23], with the only exception of the RFID tag detection mechanism that, as explained in Section III-B, can be more realistically described by a uniform probability density function with a quasi-circular symmetry around a detected tag. Note that this issue does not affect the validity of the EKF. Also, lack of stationarity is not a problem for the EKF, as it works properly even when process and measurement noises change over time, as it happens in the case considered.

Starting from these assumptions and with reference to the discrete-time system (6), the predicted state estimate at time $(k+1)T_s$ results from [33]

$$\hat{\mathbf{s}}'^{+}_{k+1} = \hat{\mathbf{s}}'_k + g(\hat{\mathbf{s}}'_k)\widehat{\boldsymbol{\Delta\Phi}}_k, \tag{13}$$

where $\hat{\mathbf{s}}'_k = [\hat{x}_k, \hat{y}_k, \hat{\theta}_k, \hat{\mu}_k, \hat{\delta}_k]^T$ is the state estimated at time kT_s. Observe that $\boldsymbol{\Gamma}_k$ is omitted in (13), because the mean value of this term is zero. The covariance matrix associated with the predicted state simply results from the linearization of (6), i.e.

$$P^+_{k+1} = F_k P_k F_k^T + G_k Q_k G_k^T + H U_k H^T, \tag{14}$$

where P_k, Q_k and U_k are the covariance matrices associated to the estimated state, to $\boldsymbol{\epsilon}_k$ and to $\boldsymbol{\Gamma}_k$, respectively; F_k is the Jacobian of the state space model with respect to $\mathbf{s}'_k$ at $[\hat{\mathbf{s}}'_k, \widehat{\boldsymbol{\Delta\Phi}}_k]$, i.e.

$$F_k = \frac{\partial[\mathbf{s}'_k + \mathbf{g}(\mathbf{s}'_k)\boldsymbol{\Delta\Phi}_k]}{\partial \mathbf{s}'_k}\Big|_{[\hat{\mathbf{s}}'_k, \widehat{\boldsymbol{\Delta\Phi}}_k]} = \\ = \begin{bmatrix} 1 & 0 & f_1 & f_2 & f_3 \\ 0 & 1 & f_4 & f_5 & f_6 \\ 0 & 0 & 1 & 0 & f_7 \\ 0 & 0 & 0 & 1 & 0 \\ 0 & 0 & 0 & 0 & 1 \end{bmatrix}, \tag{15}$$

with

$$f_1 = -c_{\widehat{\mu}_k} \sin\hat{\theta}_k(\widehat{\Delta\Phi}_{r_k} + \widehat{\Delta\Phi}_{l_k}) - Lc_{\widehat{\delta}_k} \cos\hat{\theta}_k(\widehat{\Delta\Phi}_{r_k} - \widehat{\Delta\Phi}_{l_k}),$$
$$f_2 = \frac{r}{2}\cos\hat{\theta}_k(\widehat{\Delta\Phi}_{r_k} + \widehat{\Delta\Phi}_{l_k}),$$
$$f_3 = -L\frac{r}{d}\sin\hat{\theta}_k(\widehat{\Delta\Phi}_{r_k} - \widehat{\Delta\Phi}_{l_k}),$$
$$f_4 = c_{\widehat{\mu}_k}\cos\hat{\theta}_k(\widehat{\Delta\Phi}_{r_k} + \widehat{\Delta\Phi}_{l_k}) - Lc_{\widehat{\delta}_k}\sin\hat{\theta}_k(\widehat{\Delta\Phi}_{r_k} - \widehat{\Delta\Phi}_{l_k}),$$
$$f_5 = \frac{r}{2}\sin\hat{\theta}_k(\widehat{\Delta\Phi}_{r_k} + \widehat{\Delta\Phi}_{l_k}),$$
$$f_6 = L\frac{r}{d}\cos\hat{\theta}_k(\widehat{\Delta\Phi}_{r_k} - \widehat{\Delta\Phi}_{l_k}),$$
$$f_7 = \frac{r}{d}(\widehat{\Delta\Phi}_{r_k} - \widehat{\Delta\Phi}_{l_k}).$$

and, finally, $G_k = \mathbf{g}(\hat{\mathbf{s}}'_k)$ since the model is linear with respect to the inputs.

Consider that U_k in the following will be neglected as the drift coefficients in $\boldsymbol{\Gamma}_k$ are assumed to be purely deterministic. On the contrary, Q_k depends on the performances of the chosen encoders. Since they are nominally identical, but independent, their uncertainty contributions can be assumed to be independent as well. Therefore, Q_k is a 2×2 diagonal matrix with $\sigma^2_{r_k}$ and $\sigma^2_{l_k}$ on the main diagonal. It is worth emphasizing that, to a first approximation, the standard deviation of the angular displacements measured by the right-wheel and the left-wheel encoder can be reasonably assumed to grow linearly with their respective angular velocities, i.e. $\sigma_{r_k} = \sigma_e \omega_{r_k} T_s$ and $\sigma_{l_k} = \sigma_e \omega_{l_k} T_s$.

The Kalman filter gain is then given by [33]

$$K_{k+1} = P^+_{k+1} C^T_{k+1} \left(C_{k+1} P^+_{k+1} C^T_{k+1} + D_{k+1}\right)^{-1}, \tag{16}$$

where C_{k+1} and D_{k+1} depend on the measurement data available at time $(k+1)T_s$, as explained in Section III-B. Thus, the Kalman gain (16) and the set of measurement data $\mathbf{o}_{k+1}$ collected at time $(k+1)T_s$ are used to update the system state estimate and the corresponding covariance matrix, i.e.

$$\begin{aligned} \hat{\mathbf{s}}'_{k+1} &= \hat{\mathbf{s}}'^{+}_{k+1} + K_{k+1}\left(\mathbf{o}_{k+1} - C_{k+1}\hat{\mathbf{s}}'^{+}_{k+1}\right), \\ P_{k+1} &= (I_3 - K_{k+1}C_{k+1})P^+_{k+1}. \end{aligned} \tag{17}$$

It is worth reminding that the position of the user at time kT_s is not given by $(\hat{x}_k, \hat{y}_k)$, but rather by $(\hat{x}_{u_k}, \hat{y}_{u_k})$ which is obtained by replacing $(\hat{x}_k, \hat{y}_k, \hat{\theta}_k)$ into (3).

V. Simulation-based Analysis

The accuracy of the dynamic estimator described in Section IV has been evaluated through several Monte Carlo simulations over hundreds of random paths of various length. No obstacles or walls (except for the perimeter fence) have been used to constrain the generated paths. Therefore, the performances of the algorithm have been tested in all directions and at different linear and angular velocities, i.e. for $v \in [0, 2]$ m/s and $\omega \in [-1, 1]$ rad/s. These intervals are indeed compatible with a typical human behavior. The values of the simulation parameters of encoders, gyroscope, RFID reader and camera have been obtained either from data sheets or from a preliminary characterization of the sensors and devices actually used in the development of the *c-Walker* prototype [23]. The list of such devices is reported in Section VI. For the sake of completeness, the values of the simulation parameters are listed below:

- Encoder and gyroscope sampling period: $T_s = 4$ ms;
- Standard uncertainty of encoder angular increments: $\sigma_{r_k} = 0.066\Delta\Phi_{r_k} + 0.005$ and $\sigma_{l_k} = 0.066\Delta\Phi_{l_k} + 0.005$;
- Standard deviation of the angular velocity values measured by the gyroscope (normally distributed): $\sigma_{\omega_{z_k}} = 0.15|\omega_{z_k}| + 0.08$ rad/s;
- Standard deviation of the camera-based orientation measurements (normally distributed): $\sigma_{\theta^c_k} \approx 30$ mrad, with a maximum marker detection range of 1.2 m and maximum forward angle view of 0.7 rad;
- RFID tag detection radius (circular symmetry): $R = 15$ cm with a tolerance of ± 1 cm;
- Forward velocity drift coefficient: $\mu \approx 0.015$;
- Angular velocity drift coefficient: $\delta \approx -0.01$.

The elements of the covariance matrix of the estimated state are initialized to unrealistically large values since no a-priori information is available at time 0.

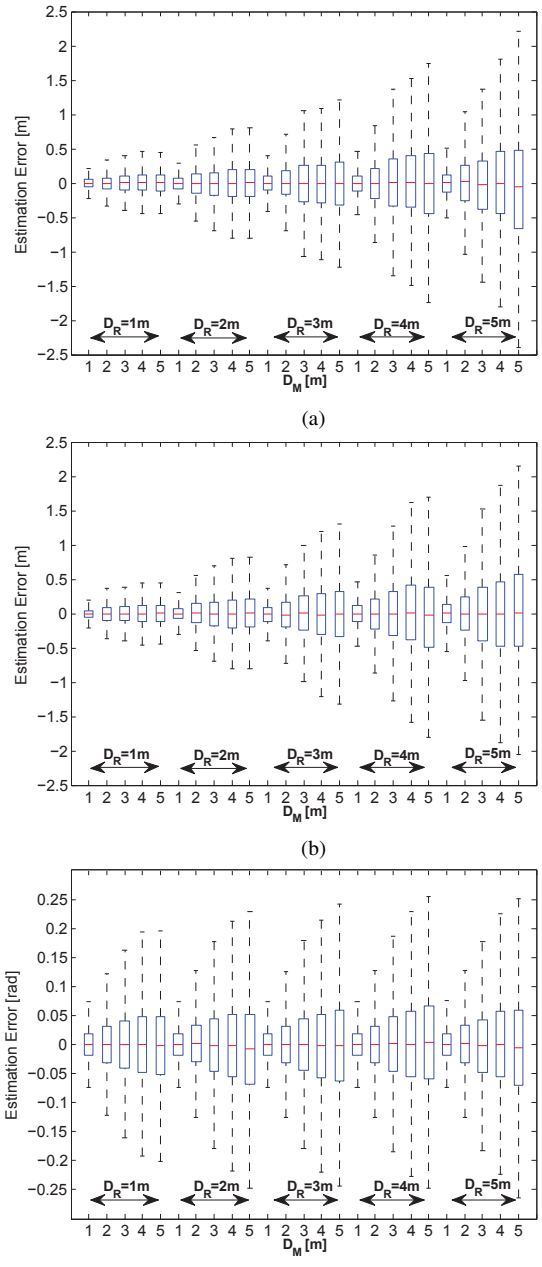

Fig. 2. Box-and-whiskers plots of x_u (a), y_u (b) and θ (c) estimation errors in 200 random trajectories, assuming to use grids of RFID tags and visual markers of different granularity [i.e. 25 pairs of (D_R, D_M) values with D_R and $D_M \in \{1, 2, 3, 4, 5\}$ m].

In the first set of simulations, 200 random trajectories of 180 s each have been generated in a large open room, assuming to use two independent grids of equally spaced tags and markers of different granularity. If D_R and D_M denote the distances between pairs of adjacent RFID tags and markers, respectively, the state estimation errors for each trajectory have been computed in 25 different configurations, obtained with both D_R and $D_M \in \{1, 2, 3, 4, 5\}$ m. Fig. 2(a)-(c) shows the box-and-whiskers plots of the x_u, y_u and θ estimation errors for different pairs of D_R and D_M. Observe that, with the chosen values of the simulation parameters, the accuracy of both position and orientation estimation degrades quite quickly as the distance between tags or markers grows. Consider also that for $D_M = 1$ m a visual marker is almost always in the reading range of the camera. Therefore, the average update rate is high, thus drastically improving performances. When either D_R or D_M ranges between 1 m and 3 m, the x_u or y_u estimation errors are generally within ± 50 cm, with a few outliers in the order of ± 1 m. Also, in the same conditions the orientation estimation errors are generally within ± 0.15 rad. Further simulation results (not shown for the sake of brevity, but qualitatively quite similar to those reported in [21]) confirm that including in the model the drift coefficients of forward and angular velocity (i.e. variables μ and δ) provides better accuracy than using an EKF with just three state variables (i.e. x, y and θ only). This result is expected since, in the latter case, the systematic, velocity-dependent uncertainty contributions due to walker asymmetries and encoders differences are not estimated and compensated. grids).

A crucial point that has to be addressed in view of deploying the proposed solution in a real environment is the optimal selection of the values of D_R and D_M. In theory, D_R and D_M should be chosen in such a way that the total number of tags and markers in the environment is minimum and the wanted position and orientation accuracy boundaries are met, as specified in Section III. Unfortunately, an analytical formalization and a solution to this optimization problem are challenging, and they deserve a study on its own, which is out of the scope of this paper. RFID tags and visual markers have a crossed random effect on EKF updates. The RFID tags are conceived to adjust position, but they also partially contribute to correct the orientation angle through the Kalman gain (16). Dually, even if the visual markers mainly adjust the estimated orientation angles, they also indirectly affect the position values. Thus, the solution to the placement optimization problem depends not only on the granularity of grids of tags and markers, taken individually, but also on their combination. The problem is further complicated by the need to define a realistic and tractable stochastic model describing user's trajectories.

In order to find a solution, at least suboptimal, to this challenging problem, a numerical approach based on Monte Carlo simulations has been adopted. The proposed procedure consists of two step. In the first one, the idea is to find the maximum values of D_R and D_M (denoted as D_{R_p} and D_{M_p}, respectively) for which the RMS position error (expressed in terms of Euclidean distance from the actual position) is smaller

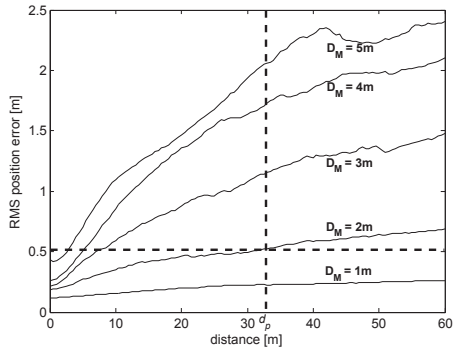

(a)

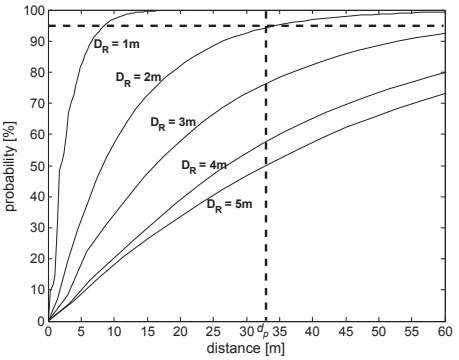

(b)

Fig. 3. (a) RMS Euclidean distances between estimated and actual positions as a function of the traveled distance when the RFID reader is disabled and $D_M \in \{1, 2, 3, 4, 5\}$ m. (b) Cumulative distribution functions associated to the probability to meet an RFID tag as a function of the traveled distance from a previous tag when $D_R \in \{1, 2, 3, 4, 5\}$ m.

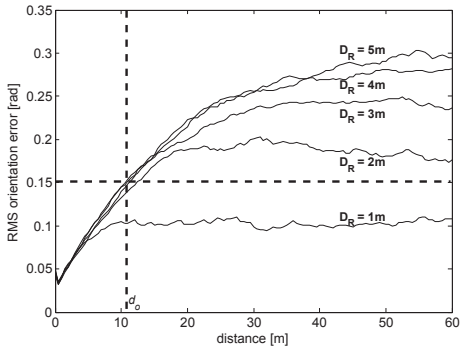

(a)

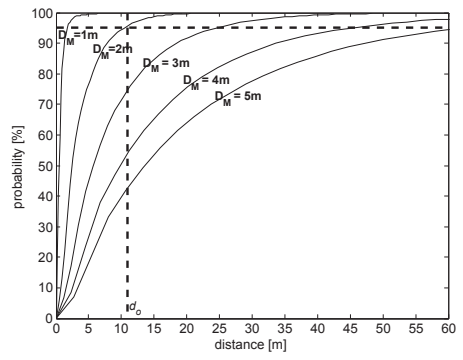

(b)

Fig. 4.

than or equal to η_p with (at least) α_p probability. In the second one, a dual approach is used to determine the maximum values of D_R and D_M (denoted as D_{R_o} and D_{M_o}, respectively) for which the RMS orientation error is smaller than or equal to η_o with (at least) α_o probability. Eventually, the suboptimal values of the distances between pairs of markers and tags can be obtained by simply choosing the more conservative solution in either step, i.e.

$$D_R^* = \min\{D_{R_p}, D_{R_o}\} \text{ and } D_M^* = \min\{D_{M_p}, D_{M_o}\}. \quad (18)$$

To address the first problem, assuming to disable the RFID reader only, the root mean square (RMS) values of the Euclidean distances between estimated and actual positions have been calculated as a function of the path length over 500 random routes for $D_M \in \{1, 2, 3, 4, 5\}$ m. The respective RMS position error curves are shown in Fig. 3(a). At the same time, the cumulative distribution functions associated to the probability for the walker to meet an RFID tag as a function of the traveled distance from a previous tag are plotted in Fig. 3(b) for $D_R \in \{1, 2, 3, 4, 5\}$ m. Fig. 3(a) allows to determine D_{M_p} and the distance d_p that the walker can cover prior to exceeding threshold η_p. Once d_p and D_{M_p} are known, the value of D_{R_p} is given by the cumulative distribution function for which the α_p-percentile of detecting an RFID tag is equal to d_p. For instance, in Fig. 3(a)-(b) the horizontal dashed lines refer to $\eta_p = 50$ cm and $\alpha_p = 95\%$, respectively. Such values meet the requirements of the DALi project. In particular, if $\eta_p = 50$ cm and $D_{M_p} \approx 2$ m, it results from Fig. 3(a) (vertical dashed line) that $d_p \approx 33$ m. Thus, it follows immediately from Fig. 3(b) that, when $d_p \approx 33$ m, then $D_{R_p} \approx 2$ m.

A dual record of Monte Carlo simulations has been performed to build the RMS orientation error curves as a function of the path length for $D_R \in \{1, 2, 3, 4, 5\}$ m, assuming that the front camera is disabled. Such curves are shown in Fig. 4(a). Also, the cumulative distribution functions associated to the probability to meet a visual marker as a function of the traveled distance from a previous marker are plotted in Fig. 4(b) for $D_M \in \{1, 2, 3, 4, 5\}$. Observe that these curves differ from those shown in Fig. 3(b), because the detection range of RFID reader and camera is also different. The approach to estimate D_{R_o} and D_{M_o} is dual to the one described above. At first, the distance d_o that the walker can cover prior to exceeding η_o and the corresponding value of D_{R_o} can be obtained from Fig. 4(a). Then, D_{M_o} can be estimated from Fig. 4(b) by finding the largest value of D_M for which the probability of meeting a marker after d_o meters is at least α_o. If, for instance, $\eta_o = 0.15$ rad and $\alpha_o = 95\%$ (also these values are compliant

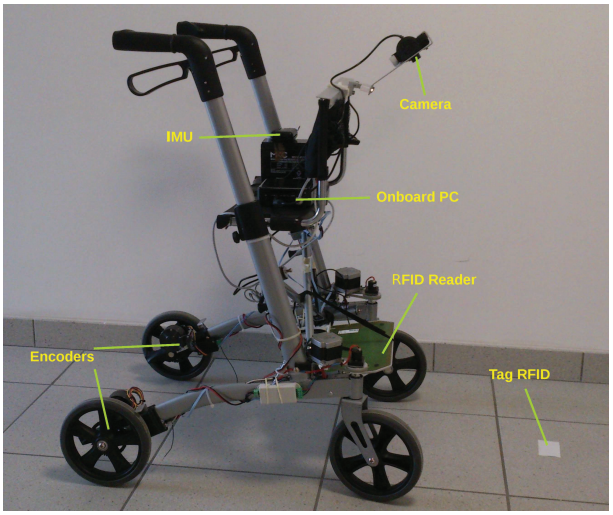

Fig. 5. The c-Walker prototype.

with the requirements of the DALi project) Fig. 4(a) shows that $d_o \approx 11$ m when $D_{R_o} \approx 5$ m. Therefore, it results from Fig. 4(b) that for the same d_o value $D_{M_o} \approx 2$ m. Ultimately, it follows from (18) that the distance between pairs of adjacent RFID tags and markers should be so conservatively set equal to $D_R^* \approx D_M^* \approx 2$ m.

VI. Implementation and Experimental Results

The position tracking algorithm described in Section III was tested on a real c-Walker prototype (Fig. 5) in the laboratories of the Department of Industrial Engineering of the University of Trento. The data from the CUI Inc. AMT10X encoders installed on the rear wheels as well as the samples from an Inversense IMU-3000 gyroscope on-board of the IMU already used in [16] are transferred to a Beaglebone embedded platform via CAN bus at 250 Hz. The Beaglebone is equipped with an AM335x ARM Cortex A8 processor running at 720 MHz and 256 MB of DDR2 RAM. The operating system on-board of the Beaglebone is a Debian Linux distribution with kernel v.3.2 patched with the RT-Preempt package to improve determinism and real-time performance. The Beaglebone collects also the data from a Feig ISC.MR101 RFID reader through a USB connection. Data acquisition and processing are implemented in C language. All the components above are powered by a 12-V 7-Ah lead-acid battery. The preprocessed measurement results, aligned on the same timescale, are transferred via Ethernet to a laptop PC equipped with a 2.26-GHz Intel Core 2 Duo processor and 2 GB of DDR2 RAM. The operating system running on the PC is a standard Ubuntu Linux. A PSeye USB webcam is linked directly to the PC and it is activated with a resolution of 640×480 pixels at a rate of just 10 Hz, to reduce both communication bandwidth requirements and computational burden. The program for visual marker recognition is implemented in C++ using the primitives of the well-known OpenCV library. The position estimation and tracking algorithm is instead implemented in C. For testing and debugging reasons, at the moment both this algorithm and the software application visualizing the motion of the c-Walker on a map run on the laptop. However, in a future version of the c-Walker they will be ported to a high-performance embedded system with a smaller form factor.

The area chosen for the experimental activities is a large room of about 300 m^2 in the basement of the Department of Industrial Engineering. The room was instrumented with RFID tags and markers put on the floor. In all experiments, $D_R^* \approx D_M^* \approx 2$ m in accordance with the simulation-based results described in Section V. All visual markers were directed as axis X_w. About 50 experiments of a different duration were conducted with the c-Walker pushed at various speeds and along different routes, both throughout the empty room and with some obstacles on the way to emulate realistic scenarios. In order to evaluate the accuracy of the position tracking technique, a laser scanner SICK S300 Expert was placed in the origin of reference frame $\langle W \rangle$ (i.e. in one corner of the room) to measure the coordinates of the user along each route in real-time. The laser scanner has an angular resolution of 0.5°, a maximum scanning angle of up to 270° (but this was limited to 90° to increase the scanning rate) and a maximum reading range of about 30 m. According to the instrument specifications, the ranging measurement accuracy depends on the size of the object and degrades as the distance from the target grows. Thus, to keep the positioning uncertainty of the laser-based system at least one order of magnitude smaller than the uncertainty of the system under test (i.e. in the order of a few cm), most of the experiments were conducted over just 150 m^2 of the available space. Also, the scanner was put on top of a 2-m-high shelf to detect just the head of the user instead of the whole c-Walker. In this way, the cluster of points collected from the scanner at a given time is quite concentrated around (x_u, y_u) and finding the position of the centroid of the cluster is simpler. The coordinates of such a centroid provide a reasonably accurate estimate of the position of the user.

Fig. 6(a)-(b) shows the results of two experiments in two possible scenarios recreated artificially in the room, i.e. the entrance hall of a shopping mall (*scenario a*) and the aisles of a supermarket (*scenario b*). The purpose of these pictures is mainly qualitative to show the correct operation of the localization system. The solid lines represent the estimated trajectories, whereas the dashed lines refer to the routes reconstructed using the scanner data. The sporadic adjustments in position or orientation due to tag or marker detection are quite evident. At a glance, the positioning uncertainty is generally well below 50 cm and always smaller than 1 m.

Fig. 7 shows the differences between the values of $\hat{x}_u$, $\hat{y}_u$, $\hat{\theta}$ estimated by the c-Walker positioning system and the corresponding values measured with the laser scanner during a travel of about 10 minutes in the empty room. The error patterns are not white, but the position uncertainty in x and y is generally well below ± 50 cm even in the long run. Similar considerations hold also for the orientation uncertainty which is generally bounded within ± 0.15 rad, as expected. The most interesting outcome of this experiment is the substantial lack of drift phenomena.

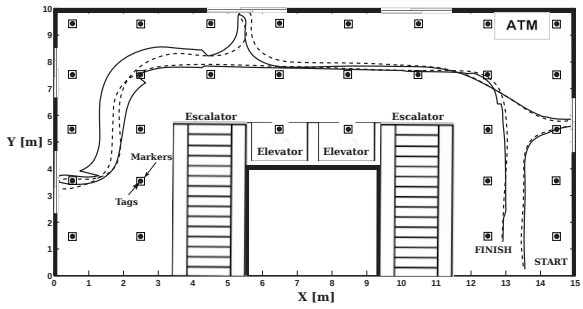

(a)

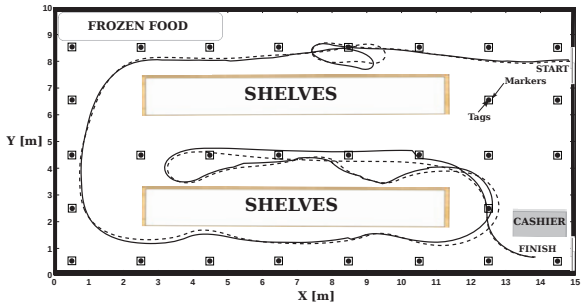

(b)

Fig. 6. Two examples of estimated trajectories (solid lines) in two different scenarios: the hall of a shopping mall (a) and some aisles of a supermarket (b). The dashed lines are the actual routes of the c-Walker reconstructed from the laser scanner data after smoothing. The uncertainty of such trajectories is in the order of a few cm.

Fig. 8 shows the histograms of the values of $\hat{x}_u - x_u$ (a), $\hat{y}_u - y_u$ (b) and $\hat{\theta} - \theta$ (c) collected in 7 further experiments. In each of them the user pushes continuously the c-Walker in all directions for at least 350 s without meeting any obstacle. Due to the quite high sampling rate (i.e. 250 Hz), the total number of data is very large, in the order of $5 \cdot 10^5$ samples. Even if the estimated probability density functions seem to be Gaussian, a more careful analysis based on normal probability plots (not reported for the sake of brevity) shows that they are not. However, all distributions are quite symmetric with mean value equal to 0 and standard deviations equal to 18 cm (for both x_u and y_u) and 0.06 rad for θ, respectively.

Finally, Table II summarizes the results of a more exhaustive characterization performed over a set of about 70 experiments of about 180 s each, with the walker moving in the room both with and without obstacles. The values in the table are the median as well as the 75th, 95th and 99th percentiles of the RMS position and orientation errors, respectively, in steady state. This is supposed to be reached after at least 2 o 3 adjustments performed through RFID tag or marker detection. Like in Section V, the individual position error values are given by the Euclidean distance between the coordinates measured by the laser scanner at a given time and the estimated trajectory at the same time. It is worth noticing that the 95th percentiles are compliant with the wanted specifications and with the results of the simulation-based design reported in Section V.

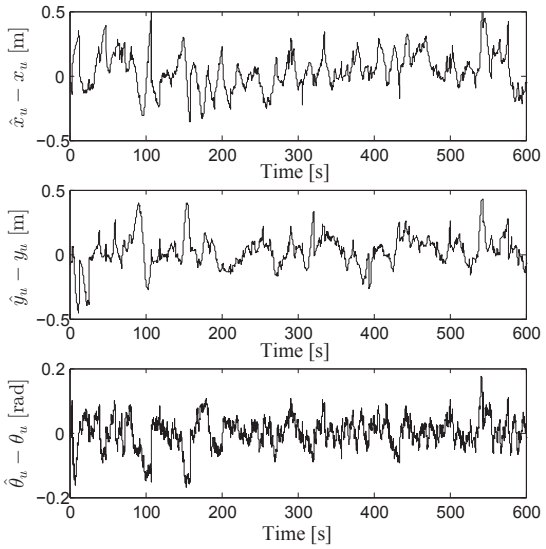

Fig. 7. Differences (as a function of time) between the values of $\hat{x}_u$, $\hat{y}_u$, $\hat{\theta}$ estimated by the c-Walker positioning system and the corresponding values measured with the laser scanner during a 10-minute long experiment.

In fact, the RMS position and orientation errors are smaller or equal to 50 cm and 0.15 rad, respectively, with at least 95% probability.

TABLE II. MEDIAN VALUE, AS WELL AS 75TH, 95TH AND 99TH PERCENTILES OF THE RMS (EUCLIDEAN) POSITION AND ORIENTATION ERRORS IN STEADY-STATE CONDITIONS OVER ABOUT 70 DIFFERENT ROUTES OF 180 S EACH.

Percentile [%]	**50**	**75**	**95**	**99**
RMS position error [cm]	40	45	50	75
RMS orientation error [rad]	0.10	0.11	0.14	0.17

VII. CONCLUSIONS

In this paper, a positioning algorithm for wheeled devices is presented and characterized experimentally. The proposed solution has been developed and implemented for a smart walker assisting older adults to navigate safely in large and complex public environments. However, it can be used with minor modifications also in different contexts, e.g. robotics. The algorithm relies on odometry and multi-sensor data fusion, namely on an extended Kalman filter (EKF) that estimates position and orientation, while compensating the angular and forward velocity systematic drifts caused by possible asymmetries or differences between left-side or right-side encoders and wheels. Passive RFID tags and simple visual markers on the floor provide accurate and sporadic adjustments in position and orientation, respectively. A conservative criterion is described to minimize the number of such devices (or, dually, to maximize the distance between them), while keeping position and orientation uncertainty within given boundaries. Compared with other RFID-based solutions, the proposed approach requires grids with a coarser granularity (i.e. less devices in the environment) and comparable performances (accuracy in the order a few tens of cm in the long run). Several

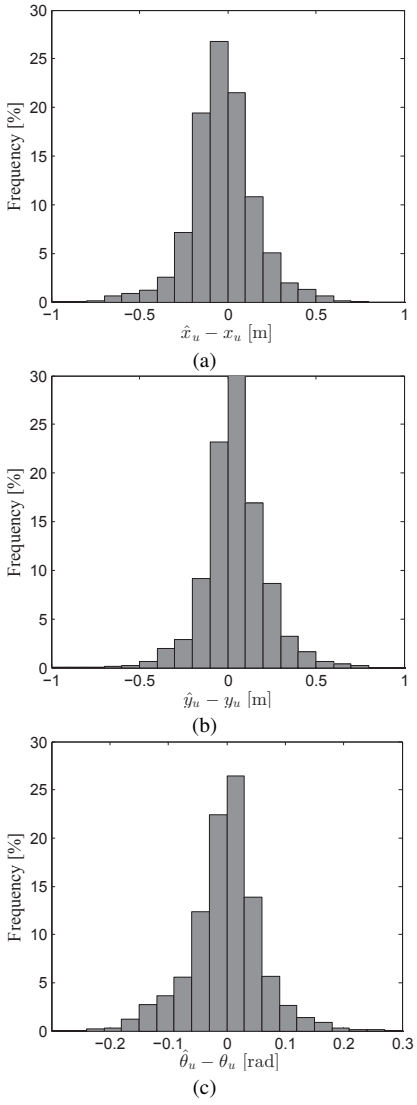

Fig. 8. Histograms of the values of $\hat{x}_u - x_u$ (a), $\hat{y}_u - y_u$ (b) and $\hat{\theta} - \theta$ (c) collected in 7 experiments of at least 350 s each.

experiments on the field confirm that the system meets such requirements with a high level of confidence.

VIII. Acknowledgments

The research work described in this paper received funding from the European Union within the 7th Framework Programme (FP7/2007-2013) under grant agreement n° ICT-2011-288917 "DALi - Devices for Assisted Living". The authors would like to thank Prof. Paolo Macchi from the Centre for Integrative Biology (CIBIO) of the University of Trento, Prof. Mariolino De Cecco, from the Department of Industrial Engineering of the University of Trento, and Dr. Michele Corrà from Tretec S.r.L., Trento, for their valuable support to the experimental activities described in this paper.

References

[1] Markets & Markets, "Indoor location market [indoor positioning and indoor navigation (IPIN); indoor mapping; indoor LBS; indoor analytics; by positioning systems (network-based, independent, hybrid)]: Global advancements, market forecasts and analysis (2013 - 2018)," 2013.

[2] S. Eisa and A. Moreira, "Requirements and metrics for location and tracking for ambient assisted living," in *Proc. International conference on Indoor Positioning and Indoor Navigation (IPIN)*, Sydney, Australia, Nov. 2012, pp. 1–7.

[3] P. Pivato, L. Palopoli, and D. Petri, "Accuracy of RSS-based centroid localization algorithms in an Indoor Environment," *IEEE Trans. on Instrumentation and Measurement*, vol. 60, no. 10, pp. 3451–3460, Oct. 2011.

[4] I. Neri, R. Centonze, M. Fravolini, and A. Moschitta, "A simple ranging technique based on received signal strength measurements in a narrowband 2.4 Ghz channel: A space diversity approach," in *Proc. IEEE Int. Workshop on Measurements and Networking Proceedings (M&N)*, Naples, Italy, Oct. 2013.

[5] D. Han, S. Jung, M. Lee, and G. Yoon, "Building a practical Wi-Fi-based indoor navigation system," *Pervasive Computing, IEEE*, vol. 13, no. 2, pp. 72–79, Apr. 2014.

[6] M. A. Stelios, A. D. Nick, M. T. Effie, K. M. Dimitris, and S. C. A. Thomopoulos, "An indoor localization platform for ambient assisted living using UWB," in *Proc. International Conference on Advances in Mobile Computing and Multimedia (MoMM)*. Linz, Austria: ACM, Nov. 2008, pp. 178–182.

[7] A. Cazzorla, G. De Angelis, A. Moschitta, M. Dionigi, F. Alimenti, and P. Carbone, "A 5.6-GHz UWB position measurement system," *IEEE Transactions on Instrumentation and Measurement*, vol. 62, no. 3, pp. 675–683, Mar. 2013.

[8] C. Rohrig and M. Muller, "Localization of sensor nodes in a wireless sensor network using the nanoLOC TRX transceiver," in *Vehicular Technology Conference (VTC)*, Apr. 2009, pp. 1 –5.

[9] H. Hur and H.-S. Ahn, "A circuit design for ranging measurement using chirp spread spectrum waveform," *IEEE Sensors Journal*, vol. 10, no. 11, pp. 1774–1778, Nov. 2010.

[10] C. De Dominicis, P. Pivato, P. Ferrari, D. Macii, E. Sisinni, and A. Flammini, "Timestamping of IEEE 802.15.4a CSS signals for wireless ranging and time synchronization," *IEEE Trans. on Instrumentation and Measurement*, vol. 62, no. 8, pp. 2286–2296, Aug. 2013.

[11] L. Angrisani, A. Baccigalupi, and R. Schiano Lo Moriello, "Ultrasonic time-of-flight estimation through unscented Kalman filter," *IEEE Transactions on Instrumentation and Measurement*, vol. 55, no. 4, pp. 1077–1084, Aug. 2006.

[12] B. Andò, S. Baglio, and C. Lombardo, "RESIMA: An assistive paradigm to support weak people in indoor environments," *IEEE Trans. on Instrumentation and Measurement*, vol. 63, no. 11, pp. 2522 – 2528, Nov. 2014.

[13] A. Bondavalli, F. Brancati, A. Ceccarelli, L. Falai, and M. Vadursi, "Resilient estimation of synchronisation uncertainty through software clocks," *Int. Journal of Critical Computer-Based Systems*, vol. 4, no. 4, pp. 301–322, Feb. 2013.

[14] E. Foxlin, "Pedestrian tracking with shoe-mounted inertial sensors," *IEEE Computer Graphics and Applications*, vol. 25, no. 6, pp. 38–46, Nov.-Dec. 2005.

[15] A. Jimenez, F. Seco, J. Prieto, and J. Guevara, "Indoor pedestrian navigation using an INS/EKF framework for yaw drift reduction and a foot-mounted IMU," in *Proc. Workkshop Positioning Navigation and Communication (WPNC)*, Dresden, Germany, Mar. 2010, pp. 135–143.

[16] A. Colombo, D. Fontanelli, D. Macii, and L. Palopoli, "Flexible indoor localization and tracking based on a wearable platform and sensor data fusion," *IEEE Trans. on Instrumentation and Measurement*, vol. 63, no. 4, pp. 864–876, Apr. 2014.

[17] R. Mautz and S. Tilch, "Survey of optical indoor positioning systems," in *Proc. Int. Conf. on Indoor Positioning and Indoor Navigation (IPIN)*, Guimarães, Portugal, Sep. 2011, pp. 1–7.

[18] N. Conci, A. Armanini, M. Daldoss, A. Colombo, D. Fontanelli, and L. Palopoli, "Wireless Sensor Networks and Video Analysis for Scalable People Tracking," in *Proc. 5th International Symposium on Communications, Control, and Signal Processing*, Rome, Italy, May 2012, pp. 1–4.

[19] L. Klingbeil, M. Romanovas, P. Schneider, M. Traechtler, and Y. Manoli, "A modular and mobile system for indoor localization," in *Proc. Int. Conf. on Indoor Positioning and Indoor Navigation (IPIN)*, Zurich, Switzerland, Sep. 2010, pp. 1–10.

[20] G. Panahandeh, M. Jansson, and S. Hutchinson, "IMU-Camera data fusion: Horizontal plane observation with explicit outlier rejection," in *Proc. International conference on Indoor Positioning and Indoor Navigation (IPIN)*, Montbeliard, France, Oct. 2013, pp. 406–414.

[21] P. Nazemzadeh, D. Fontanelli, D. Macii, and L. Palopoli, "Indoor positioning of wheeled devices for ambient assisted living: a case study," in *Proc. IEEE Int. Instrumentation and Measurement Technology Conference (I2MTC)*, Montevideo, Uruguay, May 2014.

[22] P. Nazemzadeh, D. Fontanelli, and D. Macii, "An indoor position tracking technique based on data fusion for ambient assisted living," in *Proc. IEEE Int. Conf. on Computational Intelligence and Virtual Environments for Measurement Systems and Applications (CIVEMSA)*, Milan, Italy, Jul. 2013, pp. 7–12.

[23] P. Nazemzadeh, D. Fontanelli, and D. Macii, "Design and performance analysis of an indoor position tracking technique for smart rollators," in *Proc. International conference on Indoor Positioning and Indoor Navigation (IPIN)*, Montbeliard, France, Oct. 2013, pp. 433–442.

[24] M. De Cecco, "Sensor fusion of inertial-odometric navigation as a function of the actual manoeuvres of autonomous guided vehicles," *IOP Measurement Science and Technology*, vol. 14, no. 5, pp. 643–653, May 2003.

[25] S. Park and S. Hashimoto, "Autonomous mobile robot navigation using passive RFID in indoor environment," *IEEE Trans. on Industrial Electronics*, vol. 56, no. 7, pp. 2366–2373, Jul. 2009.

[26] Byoung-Suk Choi and Ju-Jang Lee, "Sensor network based localization algorithm using fusion sensor-agent for indoor service robot," *IEEE Trans. on Consumer Electronics*, vol. 56, no. 3, pp. 1457–1465, Aug. 2010.

[27] Byoung-Suk Choi, Joon-Woo Lee, Ju-Jang Lee, and Kyoung-Taik Park, "A hierarchical algorithm for indoor mobile robot localization using RFID sensor fusion," *IEEE Trans. on Industrial Electronics*, vol. 58, no. 6, pp. 2226–2235, Jun. 2011.

[28] M. Ahmad and A. Mohan, "Novel bridge-loop reader for positioning with HF RFID under sparse tag grid," *IEEE Transactions on Industrial Electronics*, vol. 61, no. 1, pp. 555–566, Jan 2014.

[29] V. Kulyukin, A. Kutiyanawala, E. LoPresti, J. Matthews, and R. Simpson, "iWalker: Toward a rollator-mounted wayfinding system for the elderly," in *Proc. IEEE Int. Conference on RFID*, Las Vegas, NV, USA, Apr. 2008, pp. 303–311.

[30] A. A. Nazari Shirehjini, A. Yassine, and S. Shirmohammadi, "An RFID-based position and orientation measurement system for mobile objects in intelligent environments," *IEEE Trans. on Instrumentation and Measurement*, vol. 61, no. 6, pp. 1664–1675, Jun. 2012.

[31] P. Pivato, S. Dalpez, and D. Macii, "Performance evaluation of chirp spread spectrum ranging for indoor embedded navigation systems," in *Proc. IEEE Int. Symposium on Industrial Embedded Systems (SIES)*, Karlsruhe, Germany, Jun. 2012, pp. 307–310.

[32] H. Mallot, H. Blthoff, J. Little, and S. Bohrer, "Inverse perspective mapping simplifies optical flow computation and obstacle detection," *Biological Cybernetics, Springer-Verlag*, vol. 64, no. 3, pp. 177–185, Jan. 1991.

[33] Y. Bar-Shalom, X. Rong Li, and T. Kirubarajan, *Estimation with Application to Tracking and Navigation – Theory, Algorithm and Software*. John Wiley and Sons, 2001.